Gecko-Inspired Controllable Adhesive Structures Applied to Micromanipulation

Yiğit Mengüç, Sang Yoon Yang, Seok Kim, John A. Rogers, and Metin Sitti*

Gecko-inspired angled elastomer micropillars with flat or round tip endings are presented as compliant pick-and-place micromanipulators. The pillars are 35 μm in diameter, 90 μm tall, and angled at an inclination of 20°. By gently pressing the tip of a pillar to a part, the pillar adheres to it through intermolecular forces. Next, by retracting quickly, the part is picked from a given donor substrate. During transferring, the adhesion between the pillar and the part is high enough to withstand disturbances due to external forces or the weight of the part. During release of the part onto a receiver substrate, the contact area of the pillar to the part is drastically reduced by controlled vertical or shear displacement, which results in reduced adhesive forces. The maximum repeatable ratio of pick-to-release adhesive forces is measured as 39 to 1. It is found that a flat tip shape and shear displacement control provide a higher pick-to-release adhesion ratio than a round tip and vertical displacement control, respectively. A model of forces to serve as a framework for the operation of this micromanipulator is presented. Finally, demonstrations of pick-and-place manipulation of micrometer-scale silicon microplatelets and a centimeter-scale glass cover slip serve as proofs of the concept. The compliant polymer micropillars are safe for use with fragile parts, and, due to exploiting intermolecular forces, could be effective on most materials and in air, vacuum, and liquid environments.

1. Introduction

Geckos are one of Nature's most agile and power efficient climbers due to their strong, highly repeatable, high speed, and controllable attachment and detachment capabilities on a wide range of smooth and slightly rough surfaces. Such capabilities are a result of angled and hierarchical micro- and nanoscale fibrillar structures on their feet, which have saucer shaped tip

endings.[1,2] These micro/nanostructures can exhibit repeatable adhesive strengths up to 200 kPa[3,4] on smooth and rigid surfaces such as glass. The attachment strength of gecko foot-hairs was shown to be rooted in intermolecular forces such as van der Waals forces, which exist between all surfaces and are fairly insensitive to surface chemistry.[2] Such generic attachment principle enables the animal to climb on a wide range of surface materials. The importance of geometry, size, material type, and surface physics of these biological foot-hairs rather than their surface chemistry in adhesion strength leads to these biological adhesives to be called structured adhesives. Many researchers have been proposing methods to design and fabricate such synthetic micro/nanostructured adhesives inspired by gecko foot-hairs.[5–17]

In addition to high attachment strength, biological micro/nanofibrillar structures exhibit highly controllable adhesion.[1,18–23] The controlled adhesion and shear strength of gecko's angled fibrillar structures is dependent on mechanical deformations induced by vertical and lateral loading of its feet,[3,24] which can actively control the contact area between the structures and the substrate. Autumn et al.[3] demonstrated that gecko foot-hairs have a friction ratio of around 5 to 1 comparing the *with* to *against* hair tilt directions.

Synthetic structured adhesives have been designed in an attempt to mimic the strength and controllability of these biological foot-hairs. Lee and Fearing[25] showed that when initially vertical, stiff-polymer microfiber arrays are angled they exhibit anisotropic behavior of shear strength with a ratio of 45 to 1 between dragging resistance in the with and against fiber tilt directions. However, in both the vertical and angled cases, the microfibers had low adhesive strength. Zhao et al.[26] used multiwalled carbon nanotubes (MWCNTs) to create a structured surface with even smaller features that exhibit adhesion pressure of 100 kPa and shear pressure of 80 kPa. Similarly, embedding MWCNT arrays in polymer backing showed enhanced friction,[27] but these MWCNT surfaces lacked controllable adhesion.

In the study with results closest to the strength and controllability of biological foot-hairs, Murphy et al.[28] developed elastomer, angled polymer fibers with angled mushroom shaped tip

Y. Mengüç, Prof. M. Sitti
Department of Mechanical Engineering
Carnegie Mellon University
Pittsburgh, PA 15213, USA
E-mail: sitti@cmu.edu

Dr. S. Y. Yang, Prof. J. A. Rogers
Department of Materials Science and Engineering
University of Illinois at Urbana-Champaign
Urbana, IL 61801, USA

Prof. S. Kim
Department of Mechanical Science and Engineering
University of Illinois at Urbana-Champaign
Urbana, IL 61801, USA

Materials
Views

www.MaterialsViews.com

ADVANCED
FUNCTIONAL
MATERIALS

www.afm-journal.de

FULL PAPER

endings that demonstrated interfacial shear pressures of 100 kPa and adhesion pressure of 50 kPa. These structures exhibited controlled shear and adhesion strength: with-to-against shear ratios of around 5 to 1 and adhesion ratios of 35 to 1. Subsequently, surface treatments have been used to enhance adhesion of polymer microfibers in air[29] and under water.[30,31] In a different approach to adhesion control, thermal control has been used on shape memory polymer fiber arrays.[32]

The aforementioned preload-and shear-controlled adhesion and friction properties could be one of the major reasons why biological gecko foot-hairs can shed dirt particles in dry conditions.[4,33] Hansen and Autumn[4] demonstrated that dirt microparticles much larger than the fiber tip diameter could be shed from the gecko's foot after it is attached to and detached from a clean glass substrate over many cycles, a process termed contact self-cleaning. Such a property of contact self-cleaning has also been shown in synthetic polymer fiber adhesives by shear loading.[25] These studies suggest that micro/nanostructures could also be used for pick-and-place manipulation of micro- or macroscale parts since they enable controlled attachment (pick) and detachment (release). Therefore, microstructured adhesives inspired by these biological structures have recently been used for manipulation at the micro-[33,34] and macroscale.[15,35]

Kim et al.[33] presented elastomer micropyramidal structures as adhesion controlled micromanipulators. These microstructures used vertical compression induced contact area control such that there was a relatively large contact area when sufficiently large compressive loads buckled the microstructures. If pulled away quickly, a planar part was picked up with a high pull-off force because rate-dependent effects enhanced the adhesion strength further.[36] After the part was picked, the buckled elastic structures reverted to their original shapes. This shape recovery significantly reduced the contact area, and thus, adhesion, between the pyramid structures and the part and enabled easy part release. The maximum ratio of pick to release adhesive forces was 1000 to 1. However, this manipulator had small holding forces after lifting the part from the donor substrate, which could be a problem for heavy parts or for mechanical disturbances during transfer of the parts. Carlson et al.[34] addressed this limitation by removing the micropyramidal structures of the Kim et al. manipulator and used shear displacement control to reduce attachment strength at the cost of a reduced pick to release force ratio. Jeong et al.[16] utilized angled nanofibers with high shear strength to transfer a glass panel used for thin-film transistor liquid crystal displays (TFT-LCD) as a macro-scale manipulation demonstration. However, micrometer-scale part manipulation was not demonstrated and the nanofiber array required a constant application of shear force for strong adhesion.

In this study, to improve the versatility and simplicity of the elastomer micro/nanostructure based pick-and-place manipulation of macro- and microscale parts, we developed a gecko foot-hair inspired angled pillar microstructure with flat or round
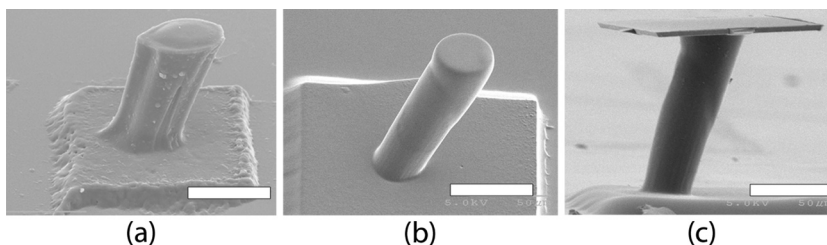

Figure 1. Scanning electron microscopy images taken from an isometric viewpoint of a) the round tip micropillar, b) the flat tip micropillar, and c) side view of the flat tip pillar attached to a silicon platelet part. The micropillars are made of elastomeric polyurethane. The white scale bars represent 50 μm of length.

tip ending shape (**Figure 1**). We present two simple control methods for reducing attachment strength of the pillar during the part release: vertical displacement control and shear displacement control. Picking of the part is accomplished in the same way for both control methods, by vertical compression of the tip to the part to maximize contact area then rapid retraction to maximize adhesion strength. During transfer of the part, the attachment between the pillar and the part is secure enough to withstand sudden impacts and disturbances as well as the weight of the part, issues that could be a limiting factor with the previously demonstrated manipulator from Kim et al.[33] During release of the part onto a receiver substrate, the contact area of the pillar to the part is drastically reduced by the deformation of the pillar due to either the vertical or shear displacement control method. As a difference from the nanofiber arrays demonstrated by Jeong et al.,[16] the parts can be picked and released in both adhesion and shear modes for the approach presented here. Such compliant micromanipulators are simple and inexpensive to manufacture, easy to integrate into optical microscopy infrastructure, and could operate in air, in vacuum, and under liquid. Finally, such compliant polymer micropillars are safe for use with fragile parts, and, due to exploiting intermolecular forces, are effective on most materials. This micromanipulation system's ease and effectiveness will be a benefit to the assembly and packaging of microelectromechanical systems and optoelectronic and flexible electronic devices.

2. Experimental Section

2.1. Fabrication

Previous work has shown the importance of the tip geometry on the adhesion and friction of microfiber adhesives.[8,37–40] To investigate the importance of tip geometry in our proposed micropillars, we used two distinct pillar types that were similar in all geometric and material parameters except for the shape of the tip. The first type has a flat tip, the surface of which is parallel to the plane of the backing layer. The second type's tip is in the shape of a rounded bump of given curvature. The principle of our fabrication methodology is based on optical lithography microstructure fabrication[41] followed by a molding based replication.[5] Angled elastomer micropillars can be fabricated by replicating positive pillars fabricated by directional reactive ion
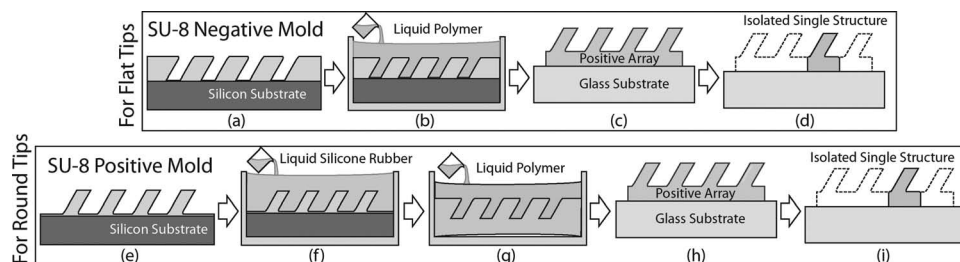
ADVANCED
FUNCTIONAL
MATERIALS
www.afm-journal.de

Materials
Views
www.MaterialsViews.com

Figure 2. Schematic representations of the fabrication process. Starting with an SU-8 negative mold (a), we could cure the liquid polymer directly (b), to produce the positive micropillar array (c), and finally select and isolate a single structure (d). Starting with an array of positive SU-8 micropillars (e), we first cured a negative silicone rubber mold (f), then cast liquid polymer (g), to produce the positive array (h), and then we isolated a single structure (i). Fabricating structures from a negative photoresist mold (a–d) results in angled pillars with flat tip endings (see Figure 1b). Replicating positive photoresist structures (f–j) results in angled pillars with round tips (see Figure 1a).

etching[16] or SU-8 lithography.[15] The latter method is selected in this study due to its simplicity.

Flat tips were formed from negative SU-8 molds because the polymer tips cure against the atomically smooth silicon wafer (**Figure 2**a). The angled flat tip micropillar fabrication process started with the patterning of an SU-8 mold. A silicon wafer was spin-coated with a 160 nm thick antireflection layer (XHRiC-16, Brewer Science). On top of the antireflection layer, SU-8 negative photoresist (SU-8 50, Microchem) was spin-coated and soft-baked into a 90 μm thick layer. To fabricate the angled pattern, the wafer with soft-baked SU-8 was mounted on an angled stage and exposed to ultraviolet (UV) light through a mask, followed by a post-exposure baking and development. The resulting SU-8 mold was a negative pattern, i.e., composed of angled holes (Figure 2a), which were hard baked at 180 °C for 3 min to induce further crosslinking. To facilitate the delamination of polydimethylsiloxane (PDMS) from the SU-8 (Supporting Information, Figure S1b), the mold was exposed to the vapor of tridecafluoro-1,1,2,2-tetrahydrooctyl-1trichlorosilane for 60 min in a dessicator.

Rounded tips are formed from positive SU-8 molds because the tips of the standing SU-8 posts are etched more along the perimeter creating a curving of the top surface (Figure 2f). By tuning the exposure and development times, the curvature can be controlled. The angled round tip micropillar used in this work was fabricated using the SU-8 lithography and molding techniques described in previous works.[15] In a similar approach to the flat tip pillar fabrication, SU-8 photoresist (SU-8 2050, Microchem Corp.) was spun on a fused silica wafer and exposed through a mask by angled UV light (MA-56, Karl Suss). The difference in round-tip fabrication from flat-tip fabrication was in the mold: the round-tip mold is a positive pattern, i.e., composed of angled pillars (Figure 2f). The SU-8 pillars were then molded with a silicone rubber (HS II RTV, Dow Corning), which served as the negative pattern mold for creating arrays of elastomer micropillars (Figure 2h). The curvature of the round tip structure was characterized with interferometric profilometry and the radius of curvature was found to be 380 μm (see Supporting Information, Figure S2).

Photolithography of SU-8 using a UV light source is a relatively accessible and established process, but it is not the only approach to producing angled polymer micro/nanostructures. Jeong et al.[16] adapted the process of deep reactive ion etching

(DRIE) to the angled etching of polysilicon. This allows for a higher degree of control and repeatability in the structures' geometry, but requires a less common fabrication technology. Conversely, we addressed the issues of consistency in SU-8 fabrication by identifying and isolating single structures with desired geometries (Supporting Information, Figure S1e–i).

The material used as the final micropillar structures was ST-1087 (BJB Enterprises, Inc.), a polyurethane elastomer with a Young's modulus of 9.8 MPa and a work of adhesion to glass of 32 mJ m^{-2}.[37] This particular polyurethane was selected for this study for the same reasons it has been used in previous similar studies: because of its high tensile strength and high surface energy while remaining optically transparent.[8,15,37] The geometry of the structures was characterized with optical microscopy (TE200 Eclipse, Nikon), interferometric profilometry (NewView™ 7300, Zygo), and scanning electron microscopy, (SEM, Hitachi 2460N). All structures were molded onto square glass plates, ≈2 mm on a side, to provide a rigid, transparent backing and to ease manual handling (Figure 2d). The molding process resulted in the plate being covered in several hundred pillars, with a polyurethane backing layer less than 20 μm thick between them and the rigid plate. This thin backing layer is advantageous because it reduces any complicating effects of the soft backing.[42]

2.2. Experimental Setup

In order to characterize the performance of the microstructures, a custom experimental system was employed. This system is based upon automated flat-punch indentation setups previously used in adhesion characterization experiments.[3,25,28,43] Using an inverted optical microscope (TE200 Eclipse, Nikon) as the base for the fixturing as well as the source of visual feedback, a vertical axis of motion and sensing was mounted such that the point of intersection between the pillar micromanipulator and substrate would occur at the focal range of the optics (Supporting Information, Figure S3). The vertical axis motion was provided by a linear motorized stage (MFA-CC, Newport) with submicrometer positional accuracy and a speed range from 1 μm s^{-1} to 2500 μm s^{-1}. The vertical stage was mounted to a two axis manual linear stage (462 Series, Newport) and a two axis goniometer (GON40-U, Newport) to align the adhesive sample with the optics and the substrate.

Materials
Views
www.MaterialsViews.com

ADVANCED
FUNCTIONAL
MATERIALS
www.afm-journal.de

FULL PAPER

Sensing was achieved through a high-resolution load cell (GSO-10 and GSO-30, Transducer Techniques), which was used with a signal conditioner (TMO-2, Transducer Techniques). The video was captured through a color digital camera (DFW-X710, Sony) connected to a desktop computer (Aspire ASE380-ED500U, Acer) operating Linux (Ubuntu 7.10 Gutsy Gibbon). The force data was captured as an analog voltage signal through a data acquisition board (NI PCI-6259, National Instruments) mounted in the computer, and all motion control was achieved through commands sent from the computer to a motor controller (ESP300, Newport) to which the motorized stage was connected. All data capture and motion control was managed by custom software running on the computer.

The experimental control parameters included the speed of approach of the adhesive sample to the substrate, the initial amount of compressive load applied (preload), the amount of displacement in the compressive direction after preloading, the amount of displacement in the lateral shear direction after preloading, and finally the pull-off speed. The variable that was measured was the applied normal force on the micropillar during loading and retraction. Visual feedback from the video recording gave qualitative information regarding the mechanics of the structures. Contact area visualization was enhanced by interference patterns in 546 nm wavelength green light.

It is important to note that the control variable in all experiments was displacement, either vertical or shear. Force-based control failed to capture intermediate load states because of the unstable nonlinear response of the pillars under compression.

2.2.1. Vertical Displacement Experiments

A typical adhesion characterization experiment would have the structural adhesive sample mounted on the vertical axis such that the adhesive was pointing downward towards the substrate mounted to the microscope fixture. After approaching at 1 μm s^{-1} (constant for all tests) and achieving a desired preload of 0.05 mN (constant for all tests) the vertical stage would continue to compress the pillar for a prescribed displacement. Once the prescribed compressive displacement was achieved, the vertical linear stage retracted the micropillar at a constant velocity. The maximum tensile force during pull-off was recorded as the adhesive force.

2.2.2. Shear Displacement Experiments

In the case of applying shear displacement during the part release, the manual linear stage was employed after the compression step was completed, but before retraction. After achieving the prescribed compressive displacement the motorized linear stage paused for 10 seconds to allow the experimenter to displace the pillar laterally through the use of the
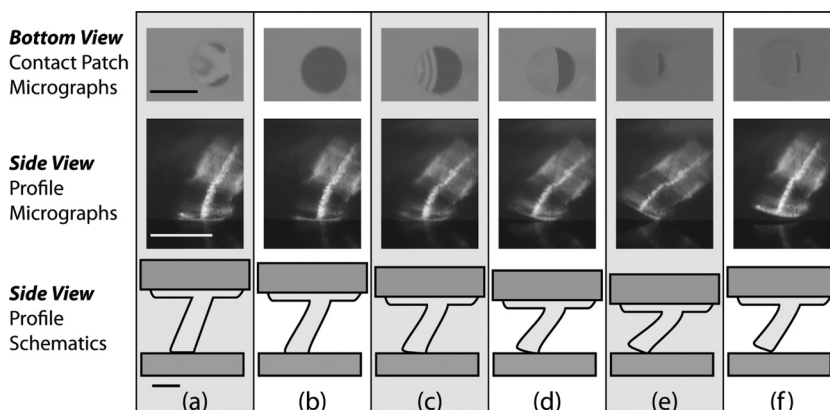

Figure 3. Each column shows three corresponding images: (top row) video stills of the flat tip pillar's contact to a smooth, flat glass as seen through an inverted microscope with monochromatic green lighting, where dark areas indicate contact; (middle row) side view video stills of the profile of the flat tip pillar as it is vertically compressed; and (bottom row) side view schematics of the pillar profile during vertical compression and retraction included in order to aid in visualizing the process. The process begins when the tip barely makes contact (a), before fully contacting the surface (b). Additional compression causes peeling due to mechanical instability (c), after which the tip continues to slide along and peel away from the surface (d,e). Upon retracting, the contact patch is seen to be minimized (f). The scale bars for each row are included in column (a) and all represent the same length: the diameter of the flat tip, 35 μm.

manual linear stage. As before, the maximum tensile force was recorded as the adhesive force.

2.2.3. Demonstration of Pick-and-Place Manipulation

A micromanipulator composed of a single angled pillar was used for all empirical characterization as well as demonstrations of pick-and-place of 100 × 100 × 3 μm³ silicon platelets. The silicon parts were fabricated according to the technique presented by Kim et al.[33] The manipulation of the centimeter-scale glass slide was conducted with an array of 100 round tip pillars arranged in a square packed pattern with 120 μm center-to-center distance.

3. Results

3.1. Effect of Tip Shape

Two micropillar geometries were investigated, one with a flat tip and one with a rounded tip. The flat tip pillar's contact process is captured in microscopy images and sketches in **Figure 3**, where the contact area microscopy images show that the "toe" (defined as the edge of the tip further away from the base of the pillar) peels up after a critical amount of compressive displacement (Figure 3c). A rounded tip pillar's contact process resembles the flat tip process, except for the lack of a critical peeling event, rather, the tip slides along the surface until the entire pillar is bent over and prone.

The behavior of these contact processes was captured quantitatively in force versus displacement graphs, shown in **Figure 4** and **Figure 5** for round and flat tips, respectively. The graphs show that there is hysteresis in the loading and
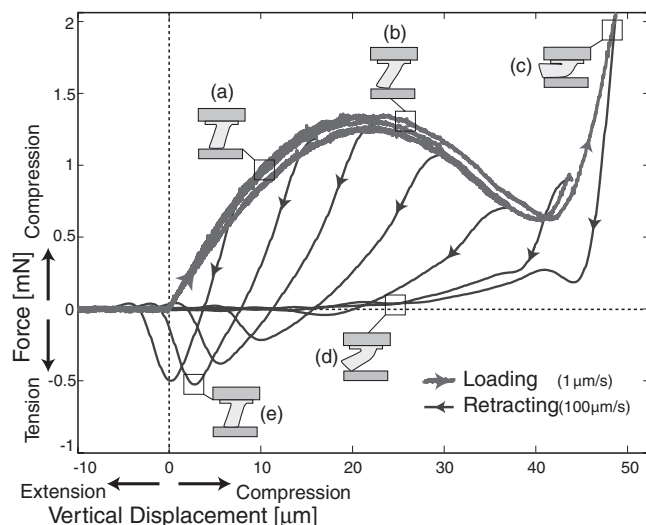
ADVANCED
FUNCTIONAL
MATERIALS
www.afm-journal.de

FULL PAPER

www.MaterialsViews.com

Figure 4. Force–distance (FD) curves of the round tip pillar obtained from indenting it onto a glass slide. FD data of the loading, at a constant compression rate of 1 μm s^{-1}, can be seen as the overlapped lines flowing from left to right. The pillar was retracted at 100 μm s^{-1} after different distances of vertical compression were obtained, which created the separate lines flowing from top right to bottom left at different intervals. The schematics of the side view of the micropillar profile are based on optical microscopy observations captured via video and correlated to the empirical FD data. The schematics show the physical behavior at points of interest along the curve, highlighted by call-out boxes. Following the FD curve from the origin (at the intersection of the dashed lines) to the point of vertical compression at (a) then retracting along the curve shows how to obtain a high adhesive force, i.e., maximum tensile force, at point (e). The adhesive force is significantly reduced if, beginning from the origin again, you compress the pillar until it is prone, as in point (c), before retracting to point (d), where we see that only edge contact is made at the moment of separation.

Figure 5. The flat tip pillar was compressed onto a glass slide at 1 μm s^{-1} then retracted at 30 μm s^{-1} to create FD curves. Loading is graphed as overlapping lines flowing from left to right, and retracting data is graphed as intermittently spaced lines flowing from the top-right to the bottom-left. The schematics of the micropillar profile are labeled to correspond directly with the information in Figure 3, and the schematics are mapped by call-out boxes to the points along the FD curve where the micropillar takes the represented shape. Compressing the pillar from the origin (the intersection of dashed lines) to gentle contact at point (a), then to point (b) before retracting to point (b)∗ gives a high adhesive force (i.e., maximum tensile force). Note that the shape of the pillar at (b)∗ is visually identical to its shape at (b), but it is in tension, so the ∗ is used to denote the difference. Compressing the pillar past (b) reveals a mechanical instability from point (c) to point (d) where the tip peels away suddenly, and by compressing even further, only the edge remains in contact at point (e) before retracting to point (f) where the pillar is making minimal contact at the moment of separation.

unloading of the micropillar that influences the pull-off force: by compressively loading the pillar, either rounded tip or flat tip, it first makes good contact resulting in high pull-off forces. Further compression causes the tip surface to peel away in the case of the flat tip, as indicated by the sharp drop in the measured compressive force seen in Figure 5c. The cause for this mechanical instability seems to be related to the nonlinear stress distribution at the tip–substrate contact face (see Supporting Information, Figure S4). In the case of the round tip pillar, the tip slowly slides until the pillar is bent and making contact on its side (Figure 4c). By controlling the vertical or shear displacement, we controlled the contact area of the pillar, and thereby control whether it is in the pick state, defined as when the pillar exerts the maximum pull-off force, or in the release state, defined as when the pull-off force is minimized.

Comparing the behavior of the flat tip pillar and round tip pillar under compression shows that the flat tip has a larger pull-off force and a sharper switch between the "pick" and "release" states, which we define as the states where we exert maximum and minimum pull-off forces, respectively. The round tip has a less sharp distinction between pick and release states, and a lower peak pull-off force. The pick-to-release adhesive force ratio of the flat tip was found to be 35 to 1 and the
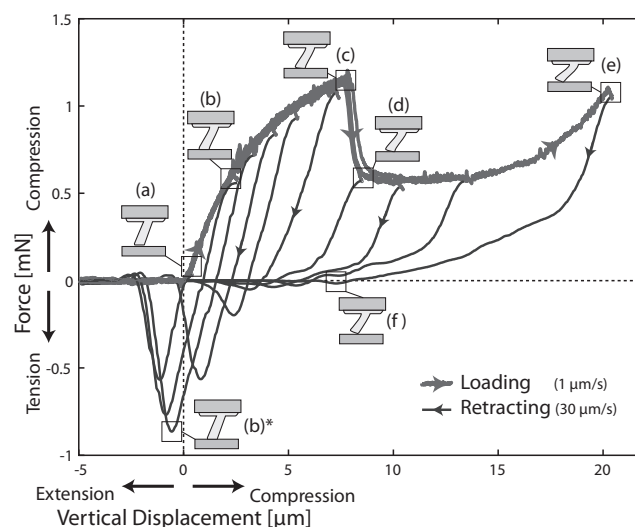
round tip had an pick-to-release adhesive force ratio of 26 to 1 (**Figure 6**).

It should be noted that the peak pull-off force of the flat tip was twice that of the round tip, but the pick-to-release adhesive force ratio of the flat tip was less than twice that of the pick-to-release ratio of the round tip because the release state of the round tip proved to exert a smaller force. It was observed that the release state depended on the roughness produced through fabrication stochasticity along the edge of the tip, and we hypothesize that deterministically adding bumps or other structures along the edge will reduce the release state adhesion and enhance the pick-to-release ratio. We observed that alignment was a factor for improving performance of the flat tip, but could be neglected for the round tip. This difference may lead to a design choice in the future for applications requiring easy or robust alignment. The higher pull-off force and sharper distinction between pick and release states leads us to use the flat tip pillar as the primary manipulator for the remainder of the work.

3.2. Effect of Shear Displacement

In a previous investigation into flat tipped angled micropillars, Aksak et al.[15] proposed an analytical model of the stress
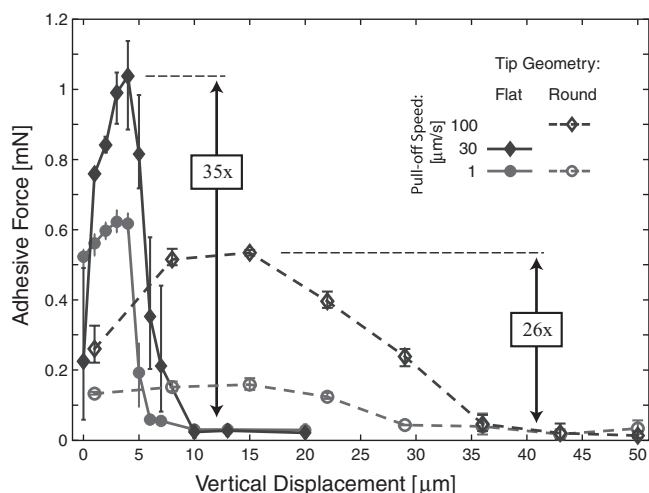
www.MaterialsViews.com

ADVANCED
FUNCTIONAL
MATERIALS
www.afm-journal.de

FULL PAPER

Figure 6. The adhesive forces of flat and round tip pillars measured during pull-off from a glass substrate, after a given vertical displacement in the compressive direction, are plotted for different retraction speeds. The slowest available retraction speed of our actuator, 1 μm s^{-1}, minimized the adhesive forces for both the flat tip pillar (solid lines connecting filled circles) and the round tip pillar (dashed lines connecting open circles). The optimal pull-off speed for the flat tip was 30 μm s^{-1} (solid lines connecting filled diamonds) and for the round tip the optimal pull-off speed was 100 μm s^{-1} (dashed lines connecting open diamonds). Each data point represents the median and the error bars indicate the minimum and maximum force values of three experiments. These results demonstrated how the flat tip pillar has a higher maximum ratio of 35 to 1 and a sharper switch between pick and release states than the round tip pillar with a maximum ratio of 26 to 1 and a smooth switch between states.

on the tip of the pillar. That model suggests that the angle of inclination of the pillar facilitates an uneven stress distribution during loading, causing the pillar to lose tip contact. We have already shown how we can maximize or minimize adhesive forces simply by loading the pillars compressively (Figure 6). However, a similar control strategy can be implemented by the addition of shear displacement. In **Figure 7**, we see that with no shearing and good tip contact, achieved after a 4 μm compression, there is a maximum pull-off force. Any amount of lateral shear displacement reduces the pull-off force until the release state is achieved for shear displacements of $\geq$8 μm. In this case, the repeatably observed pick-to-release adhesive force ratio of 39 to 1 is comparable to, but greater than, compression-only switching. From micromanipulation trials, we found that using shear displacement control of adhesion to be more repeatable and reliable than compression-only control (see Supporting Information, Video SV1).

3.3. Demonstration of Manipulation

Using the proposed vertical or shear displacement based contact area control of the micropillars, we could demonstrate pick-and-place manipulation of microparts. Such adhesion control can be seen in an assembly task in **Figure 8**, where the indentation of the pillar into the silicon microplatelet is critical for pick-and-place manipulation. With a loading condition of 4 μm of compressive displacement, the flat tip pillar tip made good
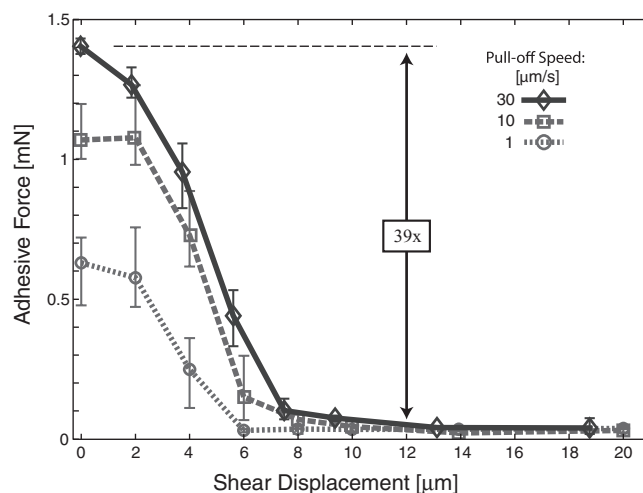

Figure 7. The adhesive forces of flat tip pillars measured at pull-off for different shear displacements and retraction speeds. Flat tip pillars were first contacted to glass with 4 μm of compression to ensure maximum tip contact, then sheared laterally before being retracted vertically at 1 μm s^{-1} (plotted with circles), 10 μm s^{-1} (squares), or 30 μm s^{-1} (diamonds). Each data point and error bars represent the median and minimum and maximum force values, respectively, of three tests. The maximum pick-to-release adhesive force ratio was found to be 39 to 1.
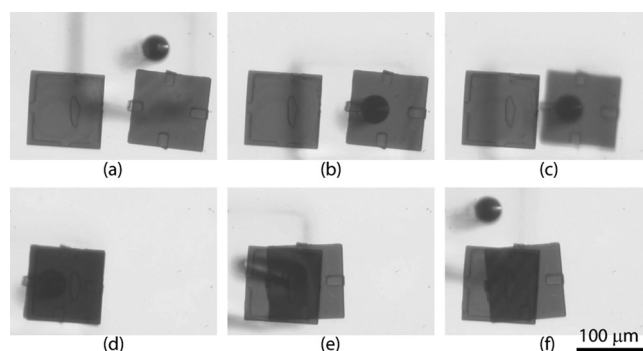

Figure 8. Video snapshots from an inverted microscope show the steps of pick-and-place manipulation of the silicon microplatelets. The micromanipulator approaches the first part (a), contacts it (b), picks it up from the substrate (c), and brings the first part in contact with the second (d). Compressive vertical displacement bends the pillar (e) and when the pillar is slowly retracted it releases the first part on top of the second, completing the microassembly (f).

contact with the part and could lift it off of the glass slide as demonstrated in Figure 8c. After moving to the desired location above the first part, the second part was released by increasing the downward displacement until the flat tip pillar lost tip contact (Figure 8e). When the pillar was retracted after tip contact was lost, the adhesion was low enough to release the second part on top of first (Figure 8f) thus beginning the assembly of a microstructure.

The same principle used to control a single angled micropillar's adhesive state can be applied to arrays of angled micropillars. A 4 $\times$ 1 cm^2 glass cover slip was picked up and placed down with a 10 $\times$ 10 array of round tip micropillars (see Supporting

ADVANCED
FUNCTIONAL
MATERIALS
www.afm-journal.de

FULL PAPER

Materials
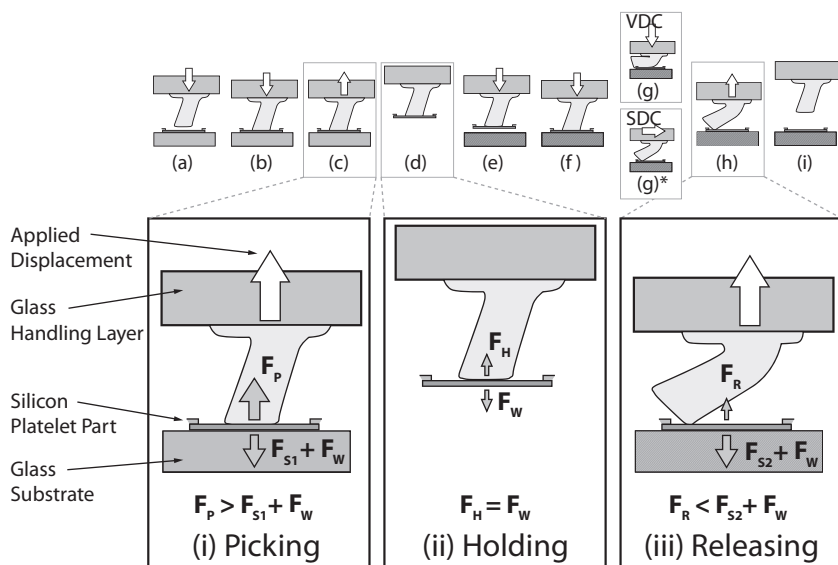Views
www.MaterialsViews.com

Figure 9. The micromanipulation process flow: a) approaching, b) contacting the part gently, c) picking up the part, d) holding while the part is transferred, e) approaching a new location or substrate, and f) bring the part into contact. To release the part we can utilize vertical displacement control (VDC) or shear displacement control (SDC). For VDC, the process begins with g) compressing until the pillar is bent and the contact area is significantly decreased, then h) retracting, and finally i) releasing the part. Utilizing SDC is identical except for the use of shear displacement (g)∗, instead of additional vertical displacement to peel the tip of the pillar. The three critical cases for manipulation are c) the picking case, d) the holding case, and h) the releasing case. The zoomed in call-outs of these three critical cases depict the forces experienced by the part because of the pillar-to-part and part-to-substrate interactions.

Information, Figure S5) demonstrating the extensibility of this approach to larger length scales and heavier parts.

4. Discussion

4.1. Picking, Holding, and Releasing Models of Manipulation

The universal van der Waals forces that act between surfaces are the roots of adhesion of the micropillar to the part and to the substrate, while the pull-off force depends on contact geometry, which we control through vertical or shear displacement. There are three conditions that are of interest to the design and implementation of a gecko-inspired pillar micromanipulator: picking, holding, and releasing conditions. From experimental results, the behavior of the microstructure under loading was observed (Figure 3), which directs us to develop an analytical expression for the critical stages of a pick-and-place manipulation process (**Figure 9**). The geometry and deformation of the pillar in response to different loading conditions controls the contact area between it and a part and consequently its pull-off force.

4.1.1. Picking

The pillar is able to pick the part up from a substrate as long as the picking force, F_P, is greater than the sum of the part to substrate adhesion, F_{S1}, and weight of the part, F_W:

$$F_P > F_{S1} + F_W \tag{1}$$

For the rounded tip, the pull-off force, P_{sphere}, is approximated to occur between a sphere and a plane,[44]

$$P_{sphere} = \frac{3}{2}\pi w_f R \tag{2}$$

where R is the radius of curvature of the tip and w_f is the work of adhesion of the interface. For the flat tip, the pull-off force, P_{flat}, is approximated as a flat punch,[45]

$$P_{flat} = \sqrt{6\pi a^3 K w_f} \tag{3}$$

where a is the radius of the flat tip, the work of adhesion of the interface is w_f, and the effective Young's modulus, K, of the system is

$$K = \frac{4}{3}\left(\frac{1-v_1^2}{E_1} + \frac{1-v_2^2}{E_2}\right)^{-1} \tag{4}$$

where v_1 and v_2 are the Poisson's ratios of the interface materials and E_1 and E_2 are the Young's moduli of the interface materials.

The picking condition also depends on viscoelastic effects, which could increase the pull-off force exerted by the pillar when retracted from a surface with a high speed (i.e., high strain rate). Viscoelastic effects can be considered to be composed of macroscale, internal, material effects, called bulk viscoelasticity, and microscale, interfacial, chemical-bond effects, called surface viscoelasticity. Bulk viscoelasticity acts to effectively stiffen the structure under rapid loading or unloading. Surface viscoelasticity modulates the effective work of adhesion. Both bulk and surface viscoelasticity can contribute to increased pull-off forces in our experimental conditions. However, due to the micrometer scale deformations of our pillar, we can ignore bulk viscoelastic effects in approximating a model of the picking condition as suggested by theory[46] and as implemented empirically in previous work.[15]

The surface viscoelasticity has been empirically shown to be related to the thermodynamic work of adhesion by a scaling factor, $w^{visco}_f(v) = \kappa(v)w_f$.[47] The scaling factor, κ, represents the relative importance between the glassy behavior of a viscoelastic material when rate of loading approaches infinity and the rubber-like behavior when rate approaches zero. Empirical evidence points to a power-law dependence by the scaling factor, κ, on retraction velocities,[48] which suggests that the scaling factor can be rewritten as $\kappa(v) = av^b + c$, where a, b, and c are empirically determined constants and v is the rate of loading. The effect of pull-off speed on pull-off force was observed to be positive for picking (Supporting Information, Figure S6), which agrees with theory.[47]

4.1.2. Holding

The holding condition can be considered to be effectively static where its governing equation is of the maximum adhesive force between a purely elastic sphere and an atomically smooth rigid

plane for the case of the rounded tip and a purely elastic cylindrical punch contacting a rigid plane for the case of the flat tip. Assuming there are no external disturbance forces, the limiting case for the holding condition is when the weight of the part, F_W, is greater than the adhesive force, F_H, and so holding is feasible only when the following inequality of forces is satisfied:

$$F_H \geq F_W \tag{5}$$

In the holding condition, we can use the non-viscoelasticity modified equations for sphere contact, Equation (2), and flat punch contact, Equation (3). High instantaneous forces allow the pillar manipulator to pick up a heavy part, but the part may fall while being transferred; so, lower pull-off speeds are a better empirical estimate of the actual holding force of the manipulator.

4.1.3. Releasing

The releasing condition resembles the picking condition in that the attraction of the part to the substrate plays a role as well as the rate at which the pillar is pulled away from the part. The objective of the releasing condition is to minimize the adhesive force between the pillar and the part, F_R, for a given combination of substrate to part adhesion, F_{S2}, and part weight F_W:

$$F_R < F_{S2} + F_W \tag{6}$$

The releasing condition for both flat tip and round tip pillars is characterized by contact along the edge, which is smaller than the picking or holding conditions. The edge contact is achieved either by vertical or shear displacement control of the pillar to induce deformation at the tip. Additionally, the pull-off speed during releasing is kept as low as possible to minimize any viscoelastic contributions to the adhesive force (see Supporting Information, Figure S3). The silicon microplatelet has a weight, F_W, that is four orders of magnitude less than the smallest measured release-state adhesive force, F_R, so the part must have an attractive force, F_{S2}, to the substrate it is being released to in order for the release to be successful.

In addition to the force inequalities, another consideration in characterizing the performance of the micromanipulator is the displacement of released parts in the direction of the pillar tilt. As the pillar with attached object is compressed into the substrate it slides and bends, which laterally displaces the part that it is carrying. An analysis of this lateral displacement showed that it was an order of tens of micrometers when the part was being released on top of a second part (Figure 8e) but on the order of micrometers or less when deposited on to a clean glass slide. The lateral displacement must be taken into account when conducting micromanipulation and assembly tasks precisely.

5. Conclusions

In this paper, we have presented an application of synthetic gecko-inspired angled elastomer micropillars to the task of manipulating and assembling parts ranging in size from micrometer to centimeter scale. These manipulators can work with only one degree of freedom actuation for part pick-and-place due to the pillar mechanical instability during vertical compression, but two degrees of freedom motion control has also been demonstrated and improves the pick-and-place performance. In addition to manipulating various parts and structures of different sizes, the manipulators can be used to assemble silicon microplatelets of planar geometry in a 2.5D assembly scheme.

Future work will seek to improve the consistency, repeatability, and fine control of the manipulation scheme. Specifically, we intend to utilize rotational stages to help orient parts and visual tracking to automate the pick and place process. Fabricating smaller pillars has been a challenge in the community, but doing so would allow for the manipulation of even smaller parts, or large parts with greater control. We anticipate that all these improvements will not only expand our ability to safely manipulate fragile microparts, but also will lend insight into the critical contact self-cleaning ability of geckos' micro/nano-hair covered feet.

[1] K. Autumn, Y. A. Liang, S. T. Hsieh, W. Zesch, W. P. Chan, T. W. Kenny, R. Fearing, R. J. Full, *Nature* **2000**, *405*, 681.
[2] K. Autumn, A. M. Peattie, *Integr. Comp. Biol.* **2002**, *42*, 1081.
[3] K. Autumn, A. Dittmore, D. Santos, M. Spenko, M. Cutkosky, *J. Exp. Biol.* **2006**, *209*, 3569.
[4] W. R. Hansen, K. Autumn, *Proc. Natl. Acad. Sci. USA* **2005**, *102*, 385.
[5] M. Sitti, R. Fearing, *J. Adhes. Sci. Technol.* **2003**, *17*, 1055.
[6] A. K. Geim, S. V. Dubonos, I. V. Grigorieva, K. S. Novoselov, A. A. Zhukov, S. Y. Shapoval, *Nat. Mater.* **2003**, *2*, 461.
[7] N. J. Glassmaker, A. Jagota, C.-Y. Hui, *Acta Biomater.* **2005**, *1*, 367.
[8] S. Kim, M. Sitti, *Appl. Phys. Lett.* **2006**, *89*, 261911.
[9] S. Kim, B. Aksak, M. Sitti, *Appl. Phys. Lett.* **2007**, *91*, 221913.
[10] C. Majidi, R. Groff, Y. Maeno, B. Schubert, S. Baek, B. Bush, R. Maboudian, N. Gravish, M. Wilkinson, K. Autumn, R. Fearing, *Phys. Rev. Lett.* **2006**, *97*, 18.
[11] H. E. Jeong, S. H. Lee, P. Kim, K. Y. Suh, *Nano Lett.* **2006**, *6*, 1508.
[12] L. Ge, S. Sethi, L. Ci, P. M. Ajayan, A. Dhinojwala, *Proc. Natl. Acad. Sci. USA* **2007**, *104*, 10792.
[13] S. Gorb, M. Varenberg, A. Peressadko, J. Tuma, *J. R. Soc. Interface* **2007**, *4*, 271.
[14] C. Greiner, A. del Campo, E. Arzt, *Langmuir* **2007**, *23*, 3495.
[15] B. Aksak, M. P. Murphy, M. Sitti, *Langmuir* **2007**, *23*, 3322.
[16] H. E. Jeong, J.-K. Lee, H. N. Kim, S. H. Moon, K. Y. Suh, *Proc. Natl. Acad. Sci. USA* **2009**, *106*, 5639.

FULL PAPER

[17] M. P. Murphy, S. Kim, M. Sitti, *ACS Appl. Mater. Interfaces* **2009**, *1*, 849.

[18] A. D. Lees, J. Hardie, *J. Exp. Biol.* **1988**, *136*, 209.

[19] S. Gorb, *Proc. R. Soc. London B* **1998**, *265*, 747.

[20] T. Eisner, D. J. Aneshansley, *Proc. Natl. Acad. Sci. USA* **2000**, *97*, 6568.

[21] W. Federle, *Integr. Comp. Biol.* **2002**, *42*, 1100.

[22] K. Autumn, M. Sitti, Y. A. Liang, A. M. Peattie, W. R. Hansen, S. Sponberg, T. W. Kenny, R. Fearing, J. N. Israelachvili, R. J. Full, *Proc. Natl. Acad. Sci. USA* **2002**, *99*, 12252.

[23] M. K. Kwak, H. E. Jeong, W. G. Bae, H.-S. Jung, K. Y. Suh, *Small* **2011**, *7*, 2296.

[24] K. Autumn, S. Hsieh, D. Dudek, J. Chen, C. Chitaphan, R. Full, *J. Exp. Biol.* **2006**, *209*, 260.

[25] J. Lee, R. S. Fearing, *Langmuir* **2008**, *24*, 10587.

[26] Y. Zhao, T. Tong, L. Delzeit, A. Kashani, M. Meyyappan, A. Majumdar, *J. Vac. Sci. Technol., B* **2006**, *24*, 331.

[27] B. Aksak, M. Sitti, A. Cassell, J. Li, M. Meyyappan, P. Callen, *Appl. Phys. Lett.* **2007**, *91*, 061906.

[28] M. P. Murphy, B. Aksak, M. Sitti, *Small* **2009**, *5*, 170.

[29] M. Sitti, B. Cusick, B. Aksak, A. Nese, H.-i. Lee, H. Dong, T. Kowalewski, K. Matyjaszewski, *ACS Appl. Mater. Interfaces* **2009**, *1*, 2277.

[30] P. Glass, H. Chung, N. R. Washburn, M. Sitti, *Langmuir* **2009**, *25*, 6607.

[31] P. Glass, H. Chung, N. R. Washburn, M. Sitti, *Langmuir* **2010**, *26*, 17357.

[32] S. Kim, M. Sitti, T. Xie, X. Xiao, *Soft Matter* **2009**, *5*, 3689.

[33] S. Kim, J. Wu, A. Carlson, S. H. Jin, A. Kovalsky, P. Glass, Z. Liu, N. Ahmed, S. L. Elgan, W. Chen, P. M. Ferreira, M. Sitti, Y. Huang, J. A. Rogers, *Proc. Natl. Acad. Sci. USA* **2010**, *107*, 17095.

[34] A. Carlson, H.-J. Kim-Lee, J. Wu, P. Elvikis, H. Cheng, A. Kovalsky, S. Elgan, Q. Yu, P. M. Ferreira, Y. Huang, K. T. Turner, J. A. Rogers, *Appl. Phys. Lett.* **2011**, *98*, 264104.

[35] H. E. Jeong, M. K. Kwak, K. Y. Suh, *Langmuir* **2010**, *26*, 2223.

[36] M. A. Meitl, Z.-T. Zhu, V. Kumar, K. J. Lee, X. Feng, Y. Y. Huang, I. Adesida, J. A. Rogers, R. G. Nuzzo, *Nat. Mater.* **2005**, *5*, 33.

[37] M. P. Murphy, B. Aksak, M. Sitti, *J. Adhes. Sci. Technol.* **2007**, *21*, 1281.

[38] A. del Campo, C. Greiner, E. Arzt, *Langmuir* **2007**, *23*, 10235.

[39] A. V. Spuskanyuk, R. M. McMeeking, V. S. Deshpande, E. Arzt, *Acta Biomater.* **2008**, *4*, 1669.

[40] D. Soto, G. Hill, A. Parness, N. Esparza, M. Cutkosky, T. Kenny, *Appl. Phys. Lett.* **2010**, *97*, 053701.

[41] Y. Xia, G. Whitesides, *Annu. Rev. Mater. Sci.* **1998**, *28*, 153.

[42] R. Long, C.-Y. Hui, S. Kim, M. Sitti, *J. Appl. Phys.* **2008**, *104*, 044301.

[43] J. Yu, S. Chary, S. Das, J. Tamelier, N. S. Pesika, K. L. Turner, J. N. Israelachvili, *Adv. Funct. Mater.* **2011**, *21*, 3010.

[44] K. Johnson, K. Kendall, A. Roberts, *Proc. R. Soc. London A* **1971**, *324*, 301.

[45] D. Maugis, *Contact, Adhesion and Rupture of Elastic Solids*, 1st ed., Springer-Verlag, Berlin **1999**.

[46] K. Shull, *Mater. Sci. Eng., R.* **2002**, *36*, 1.

[47] J. Greenwood, K. Johnson, *Philos. Mag. A* **1981**, *43*, 697.

[48] D. Maugis, M. Barquins, *J. Phys. D: Appl. Phys.* **1978**, *11*, 1989.